ELSEVIER

Journal of Alloys and Compounds 446–447 (2007) 218–223

Journal of ALLOYS AND COMPOUNDS

www.elsevier.com/locate/jallcom

# Relationship between microstructure and hydrogenation properties of $Ti_{0.85}Zr_{0.15}Mn_{1.5}V_{0.5}$ alloy

F. Cuevas [a,*], B. Villeroy [a], E. Leroy [a], P. Olier [b], M. Latroche [a]

[a] *LCMTR/CNRS, 2-8 rue Henri Dunant, 94320 THIAIS Cedex, France*
[b] *CEA/DRT/LITEN/DTNM/LTMEX, Saclay, 91191 Gif-sur-Yvette Cedex, France*

Received 13 October 2006; received in revised form 22 December 2006; accepted 30 December 2006
Available online 12 January 2007

**Abstract**

The hydrogenation properties of $Ti_{0.85}Zr_{0.15}Mn_{1.5}V_{0.5}$ alloy for four different microstructures obtained by as-cast arc melting, high-temperature annealing, ball-milling, and recrystallization after milling, have been determined. The as-cast alloy reaches a hydrogen content of 1 H/M with absorption kinetics of less than 10 s at room temperature. Sloping plateau pressures are obtained for as-cast, and annealed arc-melted alloys due to the persistence of chemical heterogeneity. Mechanical milling causes formation of amorphous phase, and improves chemical homogeneity. Milled alloy exhibits no plateau pressure, a lower hydrogen capacity (0.7 H/M), and slower kinetics. Annealing of the milled alloy at 800 °C for 30 min restores the hydrogenation capacity up to 1 H/M with a flat plateau pressure, and fast kinetics. Mechanical milling is an efficient method to obtain a chemically homogenous alloy. Subsequent annealing of the milled alloy produces homogeneous $AB_2$ crystalline phase.


*Keywords:* Intermetallics; Metal hydrides; Mechanical alloying; X-ray diffraction; Transmission electron microscopy

## 1. Introduction

Zr-based $AB_2$ Laves phases have attracted much attention as hydrogen storage materials since they absorb more than one hydrogen atom per metal atom (H/M). For instance, $ZrV_2$, $ZrCr_2$, and $ZrMn_2$ alloys absorb 1.8 H/M, 1.3 H/M, and 1.2 H/M, respectively [1]. (Ti, Zr)$Mn_2$ alloys, crystallizing in the hexagonal C14 $MgZn_2$-type structure, have particularly been studied due to reversible hydrogen absorption, easy activation, and fast kinetics under normal conditions of pressure and temperature [2–6].

Partial substitution of Zr by Ti in (Ti, Zr)$Mn_2$ alloys is technologically interesting since it allows tailoring of the plateau pressure to the required value for applications. However, significant sloping plateaux are commonly observed [2,4,6]. Fujii et al. [3] experimentally proved that sloping plateaux in (Ti, Zr)$Mn_2$ alloys are due to chemical heterogeneity. Partial substitution of Mn by other B-type elements is also beneficial to improve hydrogenation properties in terms of capacity, hysteresis, and kinetics [4–5,7–8]. Multi-substituted (Ti, Zr)(Mn, V)$_2$ alloys exhibit sloping plateaux even for well annealed samples [7–8]. Fundamental grounds rather than chemical heterogeneity have been proposed to explain this behavior [1,9].

In this work, we study the relationship between alloy microstructure and hydrogenation properties of $Ti_{0.85}Zr_{0.15}Mn_{1.5}V_{0.5}$ alloy. This compound absorbs hydrogen with fast kinetics under normal conditions [10]. Different microstructures were obtained by using four different elaboration routes, namely as-cast arc melting, high-temperature annealing, intensive milling, and recrystallization after milling. Thermodynamic and kinetic hydrogenation properties are measured, and discussed in terms of the alloy microstructure. A particular attention is paid to the study of chemical heterogeneity, and its influence on the plateau pressure.

## 2. Experimental

(Ti, Zr)(Mn, V)$_2$ alloy with nominal composition $Ti_{0.85}Zr_{0.15}Mn_{1.5}V_{0.5}$ was elaborated by arc-melting of the pure elements (minimum purity 99.7%) in a water cooled-copper crucible under argon atmosphere. The alloy was turned over, and re-melted several times to improve homogeneity. This alloy is labeled hereafter as "as-cast" alloy. Next, one part of this sample was thermally annealed at 900 °C for 21 days under argon atmosphere. This alloy is labeled hereafter as

* Corresponding author. Tel.: +33 1 4978 1225; fax: +33 1 4978 1203.
*E-mail address:* fermin.cuevas@glvt-cnrs.fr (F. Cuevas).

0925-8388/$ – see front matter © 2007 Elsevier B.V. All rights reserved.
doi:10.1016/j.jallcom.2006.12.140

Table 1
Chemical and structural characterisation for all studied alloys

| Alloy | Phase | Composition (EMPA–EDX) | Structure | $a$(Å) | $c$(Å) | $V$(Å$^3$) | V% (XRD) | V% (EMPA) |
|---|---|---|---|---|---|---|---|---|
| As-cast | $AB_2$ | $Ti_{0.84(3)}Zr_{0.16(2)}Mn_{1.50(3)}V_{0.49(2)}$ | C14 | 4.9140(4) | 8.0580(6) | 168.51(2) | 100 | 95.1 |
| | $A_3B_3O$ | Not measured | $Zr_3V_3O$ | – | – | – | Not detected | 4.9 |
| Annealed | $AB_2$ | $Ti_{0.86(4)}Zr_{0.15(4)}Mn_{1.47(2)}V_{0.51(1)}$ | C14 | 4.9157(5) | 8.060(1) | 168.66(4) | 97(1) | 94.4 |
| | $A_3B_3O$ | $Ti_{0.45}Zr_{0.05}Mn_{0.35}V_{0.15}$ | $Zr_3V_3O$ | 11.330(5) | 11.330(5) | 1454(1) | 3(1) | 5.6 |
| Milled | $AB_2$ | Not measured | C14 | 4.91(1) | 8.04(3) | 168(1) | 40[a] | – |
| | $A_3B_3O$ | Not measured | $Zr_3V_3O$ | – | – | – | Not detected | – |
| | Amorphous | Not measured | Amorphous | – | – | – | 60[a] | – |
| Recrystallized | $AB_2$ | $Ti_{0.88(6)}Zr_{0.15(3)}Mn_{1.41(5)}V_{0.53(5)}$ | C14 | 4.908(2) | 8.034(4) | 167.63(2) | 94(1) | – |
| | $A_3B_3O$ | $Ti_{0.4}Zr_{0.1}Mn_{0.4}V_{0.1}$ | $Zr_3V_3O$ | 11.36(1) | 11.36(1) | 1467(3) | 6(1) | – |

Standard deviations referred to the last significant digits are given in parentheses.
[a] Estimated value.

"annealed alloy". Mechanical grinding was done with another piece of the "as-cast" alloy. The alloy was mechanically crushed down to 1 mm, and introduced into a stainless-steal bowl under argon atmosphere. The bowl was sealed with a Taurus ring. About 8 g of alloy powder was grinded for 20 h in a planetary ball mill (Fritsch P7) at a disc rotation speed of 500 rpm with a ball-to-powder ratio of 10:1. Stainless-steal balls, 7 mm in diameter, were used. Small samples (∼300 mg in mass) were extracted at different grinding times (1.5, 5, and 20 h, respectively) for structural analyses. The alloy grinded for 20 h is labeled hereafter as "milled" alloy. A part of this alloy was annealed at 800 °C for 30 min under secondary vacuum ($10^{-6}$ Torr) and is labeled hereafter as "recrystallized" alloy.

Chemical and structural analyses were done for the four alloys (that is, "as-cast", "annealed", "milled", and "recrystallized" alloys). Chemical analyses for "as-cast" and "annealed" alloys were performed by electron probe microanalysis (EPMA) in a Cameca SX-100 instrument. Owing to its low crystallinity, chemical composition of the "recrystallized" alloy was studied by Energy Dispersive X-ray spectroscopy (EDX) in a transmission electron microscope (TEM, JEOL 2000 FX). No chemical analysis was performed for the "milled" alloy. The crystal structure of the four alloys was studied by powder X-Ray Diffraction (XRD) using Cu Kα radiation in a Bragg–Brentano θ–θ Bruker D8 Diffractomer, equipped with a backscattered rear graphite monochromator. Electron diffraction patterns for "milled" and "recrystalllized" alloys were obtained with the mentioned TEM apparatus.

Pressure-composition isotherms (PCI) and quasi-constant pressure hydrogenation kinetics of the four alloys have been measured with a Sievert's type apparatus. The samples with typical mass of 500 mg were introduced under argon atmosphere in a stainless steel container. Argon was pumped out with primary vacuum before introducing hydrogen. All hydrogenation measurements were performed at room temperature using a thermostatic bath to minimize thermal effects.

## 3. Results and discussion

### 3.1. Alloy characterization

EPMA analysis of "as-cast" and "annealed" alloys reveals that they are biphasic. The major phase exhibits $AB_2$ stoichiometry. Its composition is close to the nominal alloy value (Table 1). The minor phase has AB stoichiometry with relative Ti content much higher than that of the main phase. As will be discussed afterwards, XRD analyses indicate that the minor phase is in fact $Zr_3V_3O$-type. To illustrate EPMA results, Fig. 1 shows the titanium distribution map for both alloys. White areas correspond to the minor Ti-rich phase. The quantity of minor phase is 4.9% and 5.6%, for "as-cast" and "annealed" alloys, respectively, as determined by image analysis of Fig. 1. Its composition is about $Ti_{0.45}Zr_{0.05}Mn_{0.35}V_{0.15}$, though its fine size (∼1 μm) hampers accurate analysis by EPMA. The major phase (grey area) exhibits significant segregation with compositional gradients fluctuating along tens of microns for both alloys. Bright-grey areas are Ti- and V-rich, whereas dark grey areas are Zr- and Mn-rich. The annealing treatment changes the topological distribution between major and minor phases, but does not eliminate the chemical fluctuations within the major phase.

Fig. 2 shows EDX elemental distribution maps for all elements in one powder particle of the "recrystallized" alloy. No

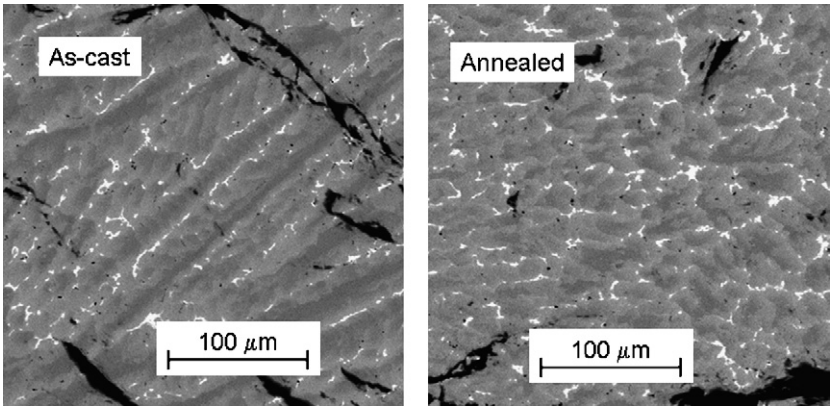


Fig. 1. Titanium distribution map of "as-cast" and "annealed" alloys obtained by EDX-TEM. White areas correspond to Ti-rich $Zr_3V_3O$-type phase. Grey areas correspond to the major $AB_2$-phase. The contrast within the grey areas reveals fluctuations in the Ti concentration. Black areas are due to sample holes and cracks.

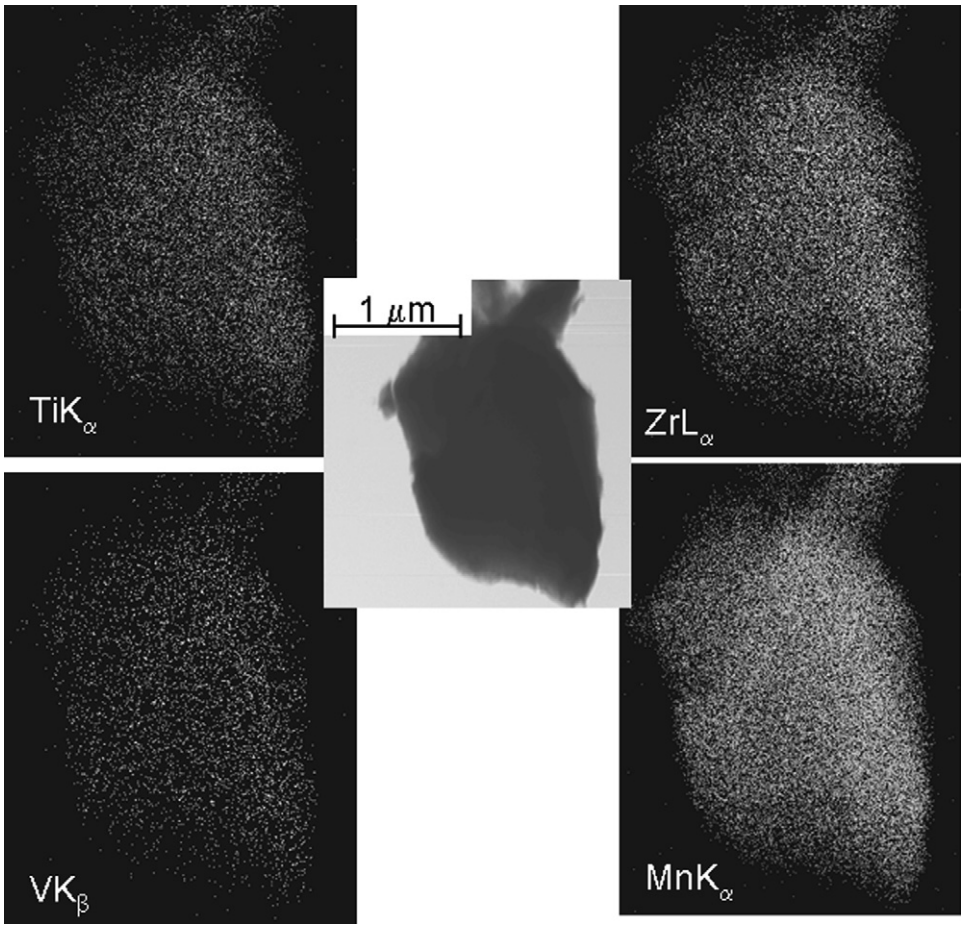


Fig. 2. Elemental distribution map and bright field image of the "recrystallized" alloy obtained by EDX.

significant chemical fluctuations are observed. The composition is consistent with $AB_2$-type phase and close to the alloy nominal value, (Table 1), except for a slight reduction of the Mn-content which can be related to partial sublimation of this element during the annealing treatment. Intensive milling followed by annealing at 800 °C produces chemically homogeneous $AB_2$-type phase. Occasionally, AB regions of composition $Ti_{0.4}Zr_{0.1}Mn_{0.3}V_{0.2}$ were detected, indicating some precipitation of the $Zr_3V_3O$-type phase.

XRD patterns for the four alloys are shown in Fig. 3. The results of XRD analysis are gathered in Table 1. All diffraction peaks from the "as-cast" alloy can be indexed to the hexagonal C14 $MgZn_2$-type structure (S.G. $P6_3/mmc$). For the "annealed" alloy, the C14-phase appears accompanied by two extra peaks. These peaks belong to the $Zr_3V_3O$-type structure (S.G. $Fd\bar{3}m$). The occurrence of this phase in V-substituting $Zr(Mn, V)_2$ alloys has already been observed by several authors [11–13]. The $Zr_3V_3O_x$ phase is stabilized by oxygen in the Zr–V system with minimum and maximum content of $0.6 \leq x \leq 1.0$, respectively [14]. This suggests that oxygen uptake from the residual atmosphere took place for the "annealed" alloy during the heat treatment leading to higher $Zr_3V_3O_x$ content for this alloy, than for the "as-cast" alloy (Table 1).

XRD pattern for the "milled" alloy exhibits a very strong peak broadening. Phase identification and characterization is better achieved after studying the evolution of XRD patterns with milling time (Fig. 4). The diffraction peaks from the C14-Laves phase are observed in all patterns. However, they broaden with milling time. Besides, two diffraction bumps centered at about 42° and 73° gradually appear. The "milled" alloy ($t = 20$ h) is then composed of both nanocrystalline-C14 and amorphous

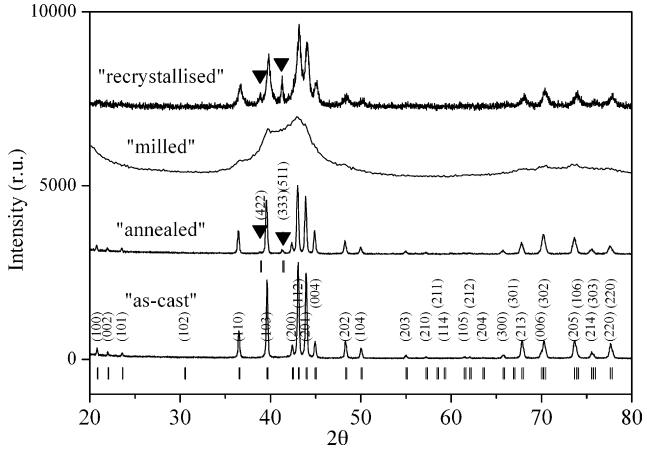


Fig. 3. XRD patterns for the four investigated alloys. Peaks from the C14-Laves phase are indexed in the "as-cast" pattern. Two detected peaks from the $Zr_3V_3O$-type phase are labeled by ▼, and indexed in the "annealed" pattern.

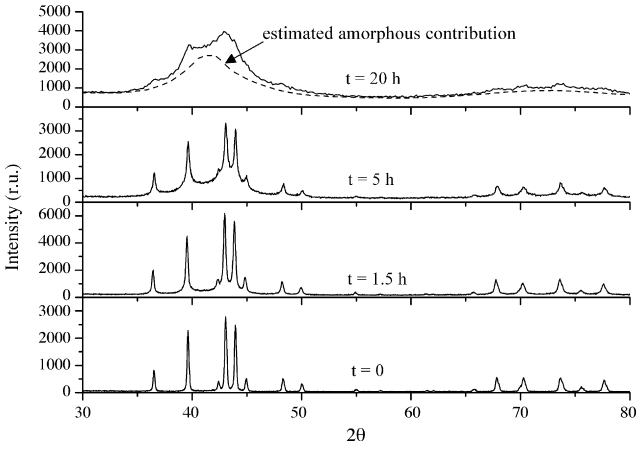


Fig. 4. XRD patterns at different milling time. For $t = 20$ h ("milled" alloy), the estimated amorphous contribution to the XRD pattern is shown by a dashed line.

phases. It is difficult to determine the quantity of amorphous phase. It is estimated to be 60% as evaluated from the ratio between the integrated intensity of the diffraction bumps (dashed line in Fig. 4), and that of the full pattern. XRD peak broadening analysis indicates that the crystallite size of the C14 nanocrystalline phase is $3.8 \pm 0.2$ nm [15]. These results are confirmed by TEM observations (left Fig. 5). The electron diffraction image for the "milled" alloy shows a wide halo, and some diffuse diffraction spots, indicating a mixture of amorphous and nanocrystalline phases, respectively. These phases are clearly observed in the dark field image (shown at the left of Fig. 5). The average crystallite size for the nanocrystalline phase is ~5 nm.

Both C14 and $Zr_3V_3O$ phases are observed in the XRD pattern for the "recrystallized" alloy (top of Fig. 3). This alloy has the highest content of $Zr_3V_3O$ phase (6% in volume as determined from the analysis of the diffraction peak intensities). This is attributed to the high reactivity of the milled powder towards residual oxygen during the thermal treatment. The C14 phase exhibits broad diffraction peaks corresponding to a crystallite size of $13 \pm 1$ nm. This is supported by TEM observations shown in Fig. 5. The electron diffraction image consists of spotty rings typical of a polycrystalline material. The dark field image shows that the "recrystallized" alloy is formed by nanocrystallites with average size of ~20 nm.

The most interesting result of this work is that homogeneous C14-Laves phase is obtained after short temperature annealing (800 °C, 30 min) of intensive milled alloy whereas an inhomogeneous one occurs after prolonged annealing (900 °C, 21 days) of arc-melted alloy. Mechanical milling decreases the crystallite size, and produces amorphous phase. This is usually achieved by continuous fracture and cold welding of alloy particles, and creation of atomic disorder [15–17]. These morphological and structural modifications tend to homogenize the alloy composition. Recrystallization of the milled alloy yields homogeneous C-14 phase. This is consistent with the results of Chuang et al. [18] and Shudo et al. [13] who report that chemically homogeneous $AB_2$-type alloys are obtained using rapid solidification techniques. Fast cooling rates allow quenching of the chemically homogeneous liquid phase.

### 3.2. Hydrogenation properties

PCI curves for the four alloys are given in Fig. 6. Hydrogen content is evaluated without considering the occurrence of the $Zr_3V_3O$-type secondary phase. The main results are gathered in Table 2. "As-cast" and "annealed" alloys exhibit quite similar isotherms with sloping plateaux for both alloys. The "as-cast" alloy has, however, a higher capacity than the "annealed"

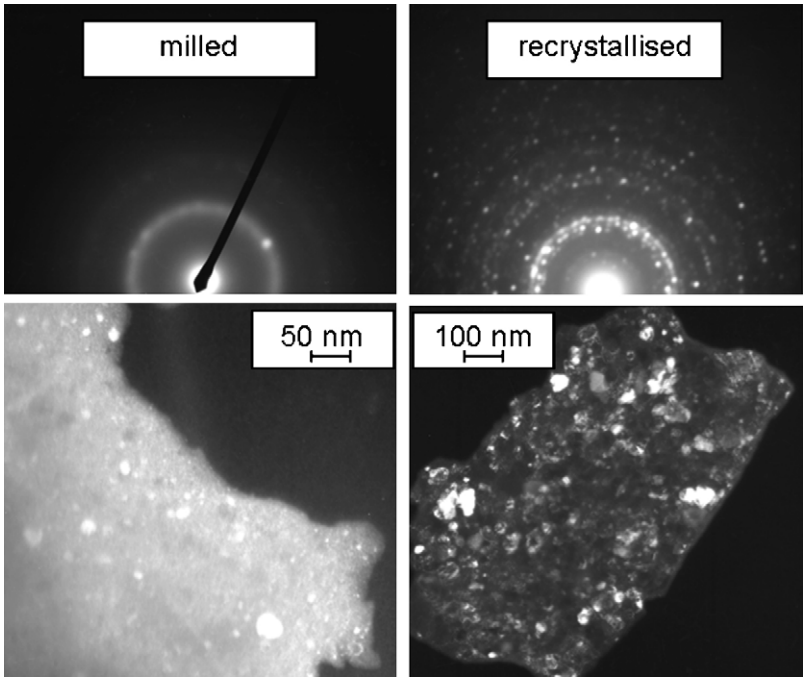


Fig. 5. Electron diffraction (top) and dark field (bottom) images of "milled" (left), and "recrystallized" (right) alloy.

Table 2
Hydrogenation properties at room temperature for the four studied alloys

| Alloy | $P$(abs)(MPa) | $P$(des) (MPa) | $C_{max}$ (H/M) | $C_{max}$ (wt%) | $C_{max}$ (g/dm$^3$) | $t_{0.8}$(abs)(s) | $t_{0.8}$(des)(s) |
|---|---|---|---|---|---|---|---|
| As-cast | 0.066 | 0.057 | 1.04 | 1.93 | 123 | 4 | 72 |
| Annealed | 0.063 | 0.057 | 1.00 | 1.85 | 118 | 5 | 79 |
| Milled | No plateau | No plateau | 0.70 | 1.29 | 82 | 148 | 810 |
| Recrystallized | 0.184 | 0.175 | 0.99 | 1.84 | 117 | 18 | 102 |

$P$ is the plateau pressure, $C_{max}$ is the maximum capacity (at ~1 MPa), $t_{0.8}$ is the time to attain 80% of the hydrogenation reaction, (abs) and (des) stand for absorption and desorption, respectively.

one (1.04 H/M as compared to 1.00 H/M), which results from its larger plateau. Loss of capacity for the annealed alloy concurs with its lower content in $AB_2$ phase. Therefore, annealing treatment of the arc-melted alloy is not only ineffective for eliminating the chemical heterogeneity, but is also detrimental for the PCI hydrogenation properties. The PCI curve for the "milled" alloy exhibits no plateau. This is attributed to the low crystallization of the alloy. Hydrogen bonding to amorphous materials occurs through a wide energy distribution [19–20]. On the contrary, a flat plateau pressure is observed for the "recrystallized" alloy after annealing. The flatness of this plateau concurs with its improved chemical homogeneity (Fig. 2). This indicates that sloping plateaux found by other authors [7–8] in multicomponent (Ti, Zr)(Mn, V)$_2$ alloys are related to the persistence of chemical heterogeneity after thermal annealing. It can be noted that the hydride of the "recrystallized" alloy is less stable (that is, it has a higher plateau pressure) than those of the "as-cast" and "annealed" alloys. This is understood from the fact that the unit-cell volume of the "recrystallized" alloy is lower than those of both "as-cast" and "annealed" alloys (Table 1). According to Lundin's geometrical model, the plateau pressure follows a linear decrease with the lattice volume for a given pseudo-binary intermetallic compound family [21–22]. The change of the cell volume between "recrystallized", and arc-melted alloys could be related to slight variations in chemical composition (Table 1).

Fig. 7 shows the absorption and desorption kinetic curves at room temperature for the four studied alloys. The time to complete 80% of reaction ($t_{0.8}$) is given in Table 2. Hydrogen absorption and desorption were conducted in all cases at hydrogen pressures close to 1 and 0.02 MPa, respectively. Very fast

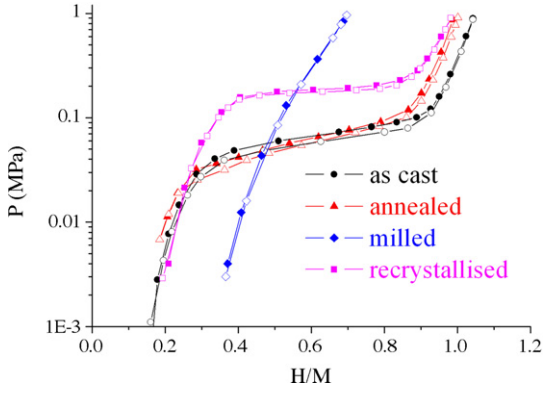


Fig. 6. PCI curves for the four investigated alloys at 25 °C. Full and empty symbols correspond to absorption and desorption data, respectively.

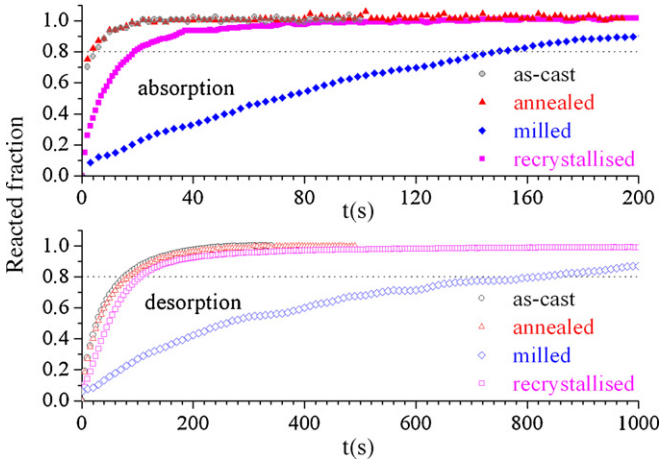


Fig. 7. Hydrogenation kinetics at 25 °C on absorption (top) and desorption (bottom) for the four studied alloys.

kinetics is observed for all alloys except for the "milled" one. Fast kinetics is related to a high diffusion coefficient for hydrogen in well-crystallized (Ti, Zr)(Mn, V)$_2$ alloys (~$10^{-7}$ cm$^2$/s at room temperature [5]). Hydrogen diffusion seems to slow down for the amorphous phase, which yields slower kinetics for the "milled" alloy. For the other three alloys, kinetics is so fast ($t_{0.8}$(abs) < 20 s) that the reaction is certainly heat transfer controlled. This concurs with the fact that hydrogenation reactions are systematically faster than dehydrogenation ones. Hydrogen absorption is exothermic, leading to sample temperature increase that accelerates, for instance, hydrogen diffusion. The opposite occurs on desorption. Nevertheless, kinetics is somehow slower for the "recrystallized" alloy than for "as-cast" and "annealed" alloys. This may be related to surface effects. For "milled" and "recrystallized" alloys, hydrogen activation was more difficult than for "as-cast" and "annealed" alloys. Milling treatment seems to produce a very active surface that is easily passivated by gaseous impurities from the residual atmosphere.

## 4. Conclusion

Room temperature PCI and kinetic hydrogenation curves of $Ti_{0.85}Zr_{0.15}Mn_{1.5}V_{0.5}$ alloy obtained by four different routes have been determined, and discussed in relation with the obtained microstructures. As-cast and annealed arc-melted alloys have very fast kinetics (80% hydrogen absorption in less than 10 s), and high hydrogen capacities (~ 1 H/M). However, both alloys exhibit sloping plateaux. The annealing treatment

does not eliminate the sloping plateau, and promotes the formation of a secondary $Zr_3V_3O$-type phase. Milling of the arc-melted alloy leads to alloy amorphisation, and improves its chemical homogeneity. Hydrogenation capacity (0.7 H/M) as well as kinetics (80% hydrogen absorption in 148 s) are poorer for the milled alloy than for arc-melted ones. However, subsequent alloy recrystallization by short time annealing at 800 °C almost restores the hydrogenation characteristics of arc-melted alloys. Furthermore, a flat plateau pressure is obtained which reflects the improved homogeneity for the main $AB_2$ phase. Mechanical milling is an efficient method to obtain chemically homogenous alloys which can be used as precursors of crystalline phases, exhibiting flat plateau pressures on hydrogen absorption/desorption.

## References

[1] D.G. Ivey, D.O. Northwood, Z. Phys. Chem. Neue Folge 147 (1986) 191–209.
[2] H. Oesterreicher, H. Bittner, Mater. Res. Bull. 13 (1978) 83–88.
[3] H. Fujii, F. Pourarian, V.K. Sinha, W.E. Wallace, J. Phys. Chem. 85 (1981) 3112–3116.
[4] T. Gamo, Y. Moriwaki, T. Yamashita, T. Iwaki, Int. J. Hydrogen Energy 10 (1985) 39–47.
[5] O. Bernauer, J. Töpler, D. Noréus, R. Hempelmann, D. Richter, Int. J. Hydrogen Energy 14 (1989) 187–200.
[6] Y. Moriwaki, T. Gamo, T. Iwaki, J. Less-Comm. Met. 172–174 (1991) 1028–1035.
[7] B.H. Liu, D.M. Kim, K.Y. Lee, J.Y. Lee, J. Alloys Compd. 240 (1996) 214–218.
[8] J.-L. Bobet, B. Darriet, Int. J. Hydrogen Energy 25 (2000) 767–772.
[9] D.G. Ivey, D.O. Northwood, J. Mater. Sci. 18 (1983) 321–347.
[10] B. Villeroy, F. Cuevas, J. Bettembourg, P. Olier, M. Latroche, J. Phys. Chem. Solids 67 (2006) 1281–1285.
[11] J.-L. Soubeyroux, L. Pontonnier, S. Miraglia, O. Isnard, D. Fruchart, E. Akiba, H. Hayakawa, S. Fujitani, I. Yonezu, Z. Phys. Chem. 179 (1993) 187–198.
[12] J. Huot, E. Akiba, H. Iba, J. Alloys Compd. 228 (1995) 181–187.
[13] Y. Shudo, H. Itoh, T. Ebisawa, J. Alloys Compd. 356–357 (2003) 497–500.
[14] F.J. Rotella, H.E. Flotow, D. Gruen, J.D. Jorgensen, J. Chem. Phys. 79 (1983) 4522–4531.
[15] J.R. Ares, F. Cuevas, A. Percheron-Guegan, Acta Mater. 53 (2005) 2157–2167.
[16] D.L. Zhang, Prog. Mater. Sci. 49 (2004) 537–560.
[17] C.C. Koch, J.D. Whittenberger, Intermetallics 4 (1996) 339–355.
[18] H.J. Chuang, S.S. Huang, C.Y. Ma, S.L.I. Chan, J.Alloys Compd. 285 (1999) 284–291.
[19] J.H. Harris, W.A. Curtin, M.A. Tenhover, Phys. Rev. B: Condens. Matter 36 (1987) 5784–5797.
[20] R. Kirchheim, Prog. Mater. Sci. 32 (1988) 261–325.
[21] C.E. Lundin, F.E. Lynch, C.B. Magee, J. Less-Comm. Met. 56 (1977) 19–37.
[22] J.-C. Achard, A. Percheron-Guégan, H. Diaz, F. Briaucourt, F. Demany, Proceedings of 2nd International Congress on Hydrogen in Metals, 1977, p. 1E12.